# Optical-field-ionized plasma x-ray lasers

D. C. Eder, P. Amendt, and S. C. Wilks
*Lawrence Livermore National Laboratory, Livermore, California 94550*
(Received 4 October 1991; revised manuscript received 16 December 1991)

A tabletop x-ray laser scheme involving lasing to the ground state of an ion following optical-field-induced ionization by a high-intensity short-pulse laser is studied. The role of the ground state in reducing the saturation intensity is calculated to be larger for H-like ions as compared with the effect in Li-like ions. Energy efficiencies of order $10^{-5}$ are calculated for the $3d_{5/2}$-$2p_{3/2}$ transition at 98 Å in Li-like Ne. The efficiency calculations are based on a driving laser with an intensity of $3\times10^{17}$ W/cm$^2$, a wavelength of 0.25 $\mu$m, a pulse duration of 100 fsec, and an input energy of 25–100 mJ. A correction to the standard stimulated Raman scattering growth rate is given for a finite laser pulse. Use of short pulses is shown to be sufficient to control heating from stimulated Raman scattering in Li-like Ne. Extending the scheme to shorter wavelengths (e.g., Li-like Al at 52 Å) is difficult because of reduced efficiencies and excessive electron heating from Raman scattering.

PACS number(s): 42.55.Vc, 32.80.Rm, 52.40.Nk, 42.65.Dr

## I. INTRODUCTION

All demonstrated x-ray lasers are based on lasing transitions between two excited states of a highly charged ion [1]. Optical-field-induced ionization by a high-intensity short-pulse laser allows for the possibility of lasing from an excited state down to the ground state of the ion. An advantage in lasing down to the ground state is the higher energy of the lasing transition as compared with lasing between excited states of the same ion. The idea of ground-state lasing following optical-field-induced ionization (which is the high-field limit of multiphoton photoionization) was considered many years ago for the case of hydrogen [2]. More recently, calculated small-sign-gain coefficients were presented for lasing down to the ground state of H-like B [3]. In this latter study, heating associated with Raman backscattering was suggested as a potential obstacle to the success of this x-ray laser scheme. Our recent calculations of heating associated with Raman backscatter show that heating can be controlled by using short driving pulses for schemes that require a laser intensity of order $10^{17}$ W/cm$^2$, e.g., Li-like Ne at 98 Å [4]. For schemes that require intensities of order $10^{18}$ W/cm$^2$, e.g., Li-like Al at 52 Å and H-like B at 48 Å, we show that it is difficult to keep heating associated with Raman backscattering at acceptable levels. The concept of lasing during recombination following multiphoton ionization has been recently demonstrated at 5080 Å in atomic cadmium [5].

The plasma conditions that are required for lasing to the ground state are a very complete emptying of the ground state prior to lasing and an electron temperature which is small compared to the ionization energy. Field ionization by a high-intensity short-pulse laser has been calculated to be an appropriate method to achieve these conditions [6–8]. (The required emptying of the ground state is difficult to achieve by using the more conventional ionization mechanisms such as collisional or radiative ionization.) The use of very short pulses ($\leq$100 fsec) gives low-energy requirements ($<1$ J) for field ionization that can be provided by tabletop laser drivers [9] and are much less than the energy requirements for most conventional x-ray laser schemes. The low-energy requirements demand a higher energy efficiency as compared with conventional x-ray laser schemes to produce a useful amount of output energy at the lasing wavelength. The amount of output energy that can be obtained from the lasing transition depends on the saturation intensity $I_{sat}$. In contrast to the standard situation of x-ray lasing between excited states, the lower laser state plays an important role in determining $I_{sat}$ when the lasing is down to the ground state. In this paper, we expand on an initial study of saturation and energy efficiencies in optical-field-ionized plasma x-ray lasers [4] and explore a number of other issues relevant to lasing down to the ground state.

In Sec. II we discuss aspects of lasing down to the ground state in H- and Li-like ions. In particular, we show the role of the lower lasing state in calculating the saturation intensity. We describe the calculation of energy efficiencies in Sec. III. In Sec. IV we present efficiencies for lasing in Li-like Ne at 98 Å for a range of initial conditions following ionization. We give details of the atomic physics calculations in Sec. V and show that the use of shell-averaged atomic data is appropriate. In Sec. VI we give a correction to the standard stimulated Raman scattering growth rate for the case of a finite laser pulse. The electron heating resulting from stimulated Raman scattering and the advantage of using short pulses are discussed. In Sec. VII we show the difficult in extending the scheme to lasing in Li-like Al at 52 Å because of reduced efficiencies and excessive Raman heating. We summarize and discuss outstanding issues in Sec. VIII.

## II. IMPORTANT ISSUES FOR LASING TO THE GROUND STATE

The two ionization stages of most interest for recombination lasing following optical-field-induced ionization

 

are H-like and Li-like ions. We use these ionization stages to illustrate a number of important issues for lasing down to the ground state. In particular, we discuss the effect of the lower lasing level in determining $I_{\rm sat}$ for a given lasing transition.

The major advantage in lasing down to the ground state is the large energy difference between the ground state and the first excited state as compared with the energy differences between excited states. In H-like ions, the $n=2$ to 1 transitions have energies about five times the energy of the $n=3$ to 2 transitions. In Li-like ions, the $n=3$ to 2 energies are about three times the $n=4$ to 3 energies and twice the $n=5$ to 3 energies. A related issue is the energy of the lasing transition as compared with the ionization potential. For transitions between excited states, Li-like ions are more "efficient," in this sense, than H-like ions. The opposite is the case for lasing down to the ground state. In H-like ions, the energy of the lasing transitions from the first excited state to the ground state is about $\frac{3}{4}$ of the ionization potential compared with $\frac{1}{2}$ the ionization potential for Li-like ions. This lower "efficiency" in Li-like ions is largely offset by using optical-field-induced ionization because the required intensity to field ionize is lower in Li-like ions for comparable ionization potentials. The threshold intensity for field ionization in H- and Li-like ions can be approximated by [8]

$$I_{\rm th}=\frac{2.2\times10^{15}}{Z^2}\left[\frac{U_i}{27.21}\right]^4 \text{ W/cm}^2 , \tag{1}$$

where $U_i$ is the ionization potential and $Z$ is the residual charge. The ionization rate associated with this threshold intensity is $10^{12}$ sec$^{-1}$. For the short pulses considered in this paper, an intensity approximately 50% higher is required to achieve the required emptying of the ground state prior to lasing. The intensity requirement for lasing in Li-like Ne is discussed in Sec. IV.

For atomic elements of interest, $I_{\rm th}$ scales with the energy of the lasing transition relatively independent of the ionization stage. We show this scaling by giving some examples for the major lasing transition in H- and Li-like ions. In H-like ions, the $2p_{3/2}$-$1s_{1/2}$ fine-structure transition has maximum gain and some examples are 135 Å and $1\times10^{17}$ W/cm$^2$ in Li, 75 Å and $6\times10^{17}$ W/cm$^2$ in Be, and 48 Å and $2\times10^{18}$ W/cm$^2$ in B. In Li-like ions, the fine-structure transition between the $n=3$ level and the $n=2$ level with the largest calculated gain coefficient is the $3d_{5/2}$-$2p_{3/2}$ transition. Some examples of wavelengths with their corresponding $I_{\rm th}$ are 128 Å and $1\times10^{17}$ W/cm$^2$ in F, 98 Å and $2\times10^{17}$ W/cm$^2$ in Ne, 52 Å and $1\times10^{18}$ W/cm$^2$ in Al, and 44 Å and $2\times10^{18}$ W/cm$^2$ in Si.

In contrast to $I_{\rm th}$, the calculation of $I_{\rm sat}$ does depend on the ionization stage. In addition, lasing down to the ground state requires that the lower state be included in the calculation of $I_{\rm sat}$. For transitions between excited states, one can often neglect the effect of the lasing intensity on the lower laser state population in calculating saturation [10]. In this case, using the definition that $I_{\rm sat}$ is the intensity at which the gain is reduced to $\frac{1}{2}$ the small-signal-gain value and neglecting the lower state in calculating gain, one has $I_{\rm sat}$ being the intensity that causes the population in the upper laser state to be reduced by a factor of 2. This intensity is found by equating the stimulated rate out of the upper laser state with the total exit rate $\gamma_{\rm out}$ excluding stimulated processes. For lasing down to the ground state, one cannot neglect the effect of the lower laser state on $I_{\rm sat}$ for two reasons. First, electrons stimulated out of the upper laser state tend to accumulate in the lower state. Second, the gain is sensitive to the population in the lower laser state because the population inversion at the time of maximum gain is not large. We first show how to calculate $I_{\rm sat}$ neglecting fine-structure levels and then discuss the role of fine structure in H-like and Li-like ions.

We introduce a parameter $\alpha$, multiplying $\gamma_{\rm out}$, whose value will depend on the populations and statistical weights of the lasing levels. We equate this product to the net stimulated emission rate out of the upper laser state,

$$\alpha\gamma_{\rm out}=\frac{c^2}{2h\nu^3}A_{ul}\left[1-\frac{N_l'g_u}{N_u'g_l}\right]J_{\rm sat} , \tag{2}$$

where $(1-N_l'g_u/N_u'g_l)$ is the population inversion factor, primes denote saturated values, $g_u$ and $g_l$ are the statistical weights for the upper and lower states, respectively, $A_{ul}$ is the spontaneous emission rate, and $J_{\rm sat}$ is the specific (per unit frequency) mean saturation intensity. The population of the upper level is reduced because of the additional exit channel via stimulated emission. By equating the outward population flow without stimulated emission $N_u\gamma_{\rm out}$ to the outward flow after saturation $N_u'\gamma_{\rm out}+N_u'\alpha\gamma_{\rm out}$, the saturated population can be expressed as $N_u'=N_u/(1+\alpha)=\beta N_u$, where $\beta\equiv1/(1+\alpha)$. Assuming that electrons arriving in the lower state accumulate there, the standard population in the lower state is $N_l'=N_l+(1-\beta)N_u$. This is usually a good approximation when the lower laser state is a ground state of the ion. (Including the small amount of recombination to the next ionization stage would result in only a modest increase in the predicted gain coefficients and saturation intensities.) The small-signal gain between the upper and lower states is

$$G_{\rm SS}=\frac{\pi e^2}{m_e c}f_{\rm osc}\Psi(\nu)N_u\left[1-\frac{N_lg_u}{N_ug_l}\right] , \tag{3}$$

where $f_{\rm osc}$ is the emission oscillator strength of the lasing transition and $\Psi(\nu)$ is the normalized line profile function. We can solve for $\beta$ requiring that the gain calculated using $N_u'$ and $N_l'$ be 0.5 times the small-signal gain giving

$$\beta=\left[\frac{1}{2}\left[1+\frac{N_lg_u}{N_ug_l}\right]+\frac{g_u}{g_l}\right]\Big/\left[1+\frac{g_u}{g_l}\right] . \tag{4}$$

Using this expression for $\beta$ to obtain $\alpha$, $N_u'$, and $N_l'$, we obtain $J_{\rm sat}$ from Eq. (2). The saturated intensity is then given by $I_{\rm sat}=\Delta\nu J_{\rm sat}(2\pi^3/\ln2)^{1/2}$, where $\Delta\nu$ is the full width at half maximum (FWHM) of the atomic line

profile.

As an example, the choice $g_u/g_l=2.25$ and $N_l g_u/N_u g_l=\frac{1}{2}$ gives $\alpha=0.09$. This results in a factor of 11 decrease in $I_{\rm sat}$ as compared with neglecting the role of the lower state in determining the intensity sufficient to saturate the laser. This choice of statistical weight corresponds to the $n=3$ and 2 levels in a Li-like ion neglecting fine structure. For lasing down to the ground state of a H-like ion from the first excited state, $g_u/g_l=4$ and $\alpha=0.05$ for the same amount of inversion.

The spacing between the fine-structure levels of interest is often greater than the linewidths of the lasing transitions and the effects of fine structure must be included in calculating saturation. The assumption that the fine-structure levels are populated according to their statistical weights allows an easy estimate of the role of fine structure on saturation. We show the validity of this approximation in Sec. V. In Li-like ions, the $3d_{5/2}$-$2p_{3/2}$ transition is calculated to be the first fine-structure transition between the $n=3$ and 2 levels to reach saturation. In Eq. (2) we use the spontaneous emission rate $A_{ul}$ for this fine-structure transition, but we continue to use the shell-averaged or total exit rate $\gamma_{\rm out}$. The outward population flow without stimulated emission is $N_{n=3}\gamma_{\rm out}=3N_u\gamma_{\rm out}$, where $N_u$ is the population of the $3d_{5/2}$ upper laser level which has $\frac{1}{3}$ of the $n=3$ population if the sublevels are populated according to their statistical weights. Equating this to the outward flow after saturation, $3N_u'\gamma_{\rm out}+N_u'\alpha\gamma_{\rm out}$, one obtains an expression for $N_u'$ given by $N_u'=N_u/(1+\alpha/3)=\tilde{\beta}N_u$, where $\tilde{\beta}\equiv 1/(1+\alpha/3)$. (If the lower state is neglected in calculating saturation, $\alpha=3$ because the stimulated rate acts only on the $3d_{5/2}$ population.) Assuming that electrons that are stimulated out of the $3d_{5/2}$ level into the $2p_{3/2}$ level are distributed between the $n=2$ fine-structure levels according to their statistical weights, one obtains $N_l'=N_l+\frac{1}{2}(1-\tilde{\beta})N_u$. Using the definition of $I_{\rm sat}$, we find

$$\tilde{\beta}=\left[\frac{1}{2}\left[1+\frac{N_l g_u}{N_u g_l}\right]+\frac{1}{2}\frac{g_u}{g_l}\right]\Bigg/\left[1+\frac{1}{2}\frac{g_u}{g_l}\right]. \quad (5)$$

For $g_u/g_l=6/4=1.5$, appropriate for the $3d_{5/2}$-$2p_{3/2}$ transition, and $N_l g_u/N_u g_l=1/2$ one calculates that $\alpha=0.5$. Thus, including the lower state results in a factor of 6 decrease in $I_{\rm sat}$ for the assumed inversion.

In H-like ions, the $2p_{3/2}$-$1s_{1/2}$ transition has the largest gain coefficient and saturates first. The $2p_{3/2}$ level has $\frac{1}{2}$ of the $n=2$ population if the sublevels are populated according to their statistical weights and we have $N_u'=N_u/(1+\alpha/2)=\hat{\beta}N_u$ and $N_l'=N_l+(1-\hat{\beta})N_u$. These are the same expressions as for the first case, where fine structure is neglected, with $\hat{\beta}$ replacing $\beta$. The expression for $\beta$, Eq. (4), can be used for $\hat{\beta}$ with $\alpha=2(1/\hat{\beta}-1)$. For $g_u/g_l=2$, appropriate for the $2p_{3/2}$-$1s_{1/2}$ transition, and $N_l g_u/N_u g_l=1/2$ one calculates $\alpha=0.18$, which is a factor of 11 smaller as compared with neglecting the lower state population. For comparable population inversions, the $2p_{3/2}$-$1s_{1/2}$ transition in H-like ions has a greater reduction in $I_{\rm sat}$, associated with including the lower laser state, than the $3d_{5/2}$-$2p_{3/2}$ transition in Li-like ions.

## III. CALCULATION OF EFFICIENCIES

A major question in determining the usefulness of optical-field-ionized plasma x-ray lasers is the amount of output energy $E_{\rm out}$ in lasing transition compared with the required input energy $E_{\rm in}$. We define an efficiency $\eta$ as the ratio of these energies $\eta\equiv E_{\rm out}/E_{\rm in}$. The low-energy requirements of optical-field-ionized plasma x-ray lasers, as compared with conventional x-ray laser schemes, demand a higher efficiency to produce a useful amount of output energy at the lasing wavelength. The required efficiency depends on several factors, such as type of application, repetition rate, and laser driver cost. Efficiencies larger than $10^{-6}$, representative of conventional x-ray laser efficiencies, are desired for optical-field-ionized plasma x-ray lasers. A potential x-ray laser with such efficiencies is discussed in the next section.

The driving or ionizing laser creates a cylindrical lasing medium with a radius approximately equal to the laser half-intensity radius. The $z$ axis of the cylinder is aligned along the propagation direction of the laser. The length of the lasing medium is determined by the distance that the pulse travels with the intensity above $I_{\rm th}$ for the appropriate ions species. Refraction, diffraction, and energy absorption serve to limit the length. The ionization at the leading edge of the pulse creates a transverse electron density profile that can spread the beam resulting in a very short lasing medium. Creating a plasma waveguide by using a prepulse has been proposed as a solution to this refraction problem [3]. In this paper, we consider only the effects of diffraction and energy absorption assuming that the length of the lasing region is given by the confocal length [11]

$$L_{\rm cf}=4\pi a^2/\lambda \ln 2 , \quad (6)$$

where $\lambda$ is the wavelength of the driving laser. We require that there be sufficient energy in the pulse to ionize the plasma for a confocal length. To ionize a Ne gas to He-like Ne with an electron density of $5\times10^{20}$ cm$^{-3}$ in a cylindrical volume of length 0.7 cm and radius 10 $\mu$m requires 20 mJ. This is approximately $\frac{1}{5}$ of the energy in a 100-fsec pulse with a 10-$\mu$m half-intensity radius and an intensity of $3\times10^{17}$ W/cm$^2$. This requirement provides a limit on the increase in length that can be obtained by increasing the focal radius. For a fixed driving wavelength and intensity, the efficiency for a saturated laser is proportional to $a^2(I_{\rm sat}/L_{\rm sat})(\Delta t/\tau_{\rm FWHM})$, where $\tau_{\rm FWHM}$ is the FWHM duration of the driving laser. We show the dependence of $I_{\rm sat}$, $L_{\rm sat}$, and $\Delta t$ on electron density and temperature in the following section for the case of Li-like Ne.

The x-ray laser pulse follows behind the ionizing pulse with a delay determined by the time required to achieve maximum gain after ionization, which is independent of $z$, and by plasma dispersion. The formulas in this paper assume that the uv ionizing pulse and the following x-ray laser pulse travel through the plasma at the same speed.

Plasma dispersion causes the x-ray pulse to travel faster than the uv pulse with the ratio of the velocities approximately $(1-n_e/n_{cr})^{1/2}$, where $n_{cr}$ is the critical density for the uv light. For $n_e=5\times10^{20}$ cm$^{-3}$ and $\lambda=0.25$ $\mu$m, the difference in transit time for 1 cm is 0.48 psec. This is of the order of the FWHM gain duration, calculated in Sec. IV, for lasing in Li-like Ne. Therefore we restrict our attention to plasma radii less than or equal to 10 $\mu$m ($z\leq 0.7$ cm).

In order to calculate the output energy and resulting efficiency we must determine the distance along the laser (or $z$ axis) at which the amplifying intensity reaches $I_{sat}$; this condition defines the saturation length $L_{sat}$. The saturation length is found by equating $J_{sat}$, Eq. (2), with the line mean (or Gaussian line profile weighted) intensity $J$ at $z=L_{sat}$:

$$J=S\left[\int_0^{\tan^{-1}(a/L_{sat})}\frac{(e^{GL_{sat}/\cos\theta}-1)^{3/2}}{[(GL_{sat}/\cos\theta)e^{GL_{sat}/\cos\theta}]^{1/2}}\sin\theta d\theta+\int_{\tan^{-1}(a/L_{sat})}^{\pi/2}\frac{(e^{Ga/\sin\theta}-1)^{3/2}}{[(Ga/\sin\theta)e^{Ga/\sin\theta}]^{1/2}}\sin\theta d\theta\right], \tag{7}$$

where $S=(2h\nu^3/c^2)/(1-N_lg_u/N_ug_l)$ is the source function, $G$ is the gain, $a$ is the lasing medium half-width or half-intensity radius, and $\theta$ is the angle from the $z$ axis at which the (geometric) ray propagates through the plasma. The integrands in Eq. (7) together represent the line integrated specific intensity which is found by first solving the line transfer equation for the specific intensity $I(\nu)$, weighting $I(\nu)$ by a line profile function which we take as Gaussian, and then integrating over frequency [10]. The first integral corresponds to rays which exit the end of the lasant medium at $z=L_{sat}$, and the second includes contributions from rays which exit from the side of the slab ($z<L_{sat}$). In most treatments of x-ray lasers, one assumes that $a\ll L_{sat}$ as well as an intensity scaling of $\exp(GL)/\sqrt{GL}$ for large gain lengths. In this limit, the second integral drops out and Eq. (7) reduces to $J=(S/2)[\exp(GL_{sat})/(GL_{sat})^{1/2}](a^2/L_{sat}^2)$. However, the x-ray laser presented here can often have very large gains (particularly at low electron temperatures), thereby having $a\not\ll L_{sat}$. Therefore we are generally required to include the contribution from rays exiting the sides of the lasant plasma as embodied in the second integral of Eq. (7). We arbitrarily choose to exclude those solutions for $L_{sat}$ which are less than $\sim 20a$ in order to have an x-ray source with highly directed output.

The intensity of the laser increases exponentially with length until saturation is reached, whereupon the dependence on length becomes nearly linear. A good approximation to this dependence of the intensity on the length of the lasing medium is

$$I(z)=\begin{cases}\dfrac{I_{sat}(e^{Gz}-1)^{3/2}(GL_{sat}e^{GL_{sat}})^{1/2}}{(Gze^{Gz})^{1/2}(e^{GL_{sat}}-1)^{3/2}} & \text{if } z<L_{sat}\\ I_{sat}\dfrac{z}{L_{sat}} & \text{if } z\geq I_{sat}\ .\end{cases} \tag{8}$$

For a given length of the lasing medium $z$ and duration of lasing $\Delta t$ [where we take $\Delta t$ as the temporal duration (FWHM) of the calculated gain coefficient for the lasing transition], the output energy can be written as $E_{out}=I(z)\Delta t\pi a^2$.

The efficiencies, discussed above and presented in the following sections, are the ratio of total output energy divided by the input energy. Some applications of x-ray lasers, such as holography of living cells, require a coherent source of x rays. The longitudinal (temporal) coherence is expressed in terms of a longitudinal coherence length $L_l$ defined as the distance over which phase is maintained: $L_l=\lambda_x^2/\Delta\lambda_x$, where $\lambda_x$ is the wavelength of the x-ray lasing transition and $\Delta\lambda_x$ is the lasing transition linewidth. In Li-like Ne, the linewidth of the $3d_{5/2}$-$2p_{3/2}$ transition is primarily determined by Stark broadening [12], and we calculate $L_l\approx 60$ $\mu$m for an electron density of $5\times10^{20}$ cm$^{-3}$. This degree of longitudinal coherence is sufficient for most applications. Transverse (spatial) coherence is more problematic for the scheme proposed in this paper and for demonstrated x-ray laser schemes [13]. The transverse coherence length $L_t$ can be approximated as $L_t\approx a/F$, where $F=2\pi a^2/(\lambda_x z)$ is the Fresnel number. The number of saturated transverse modes scales as the square of the Fresnel number, and the fraction of output energy which is coherent scales as $1/F^2$. If the lasing length $z$ is given by $L_{cf}$, Eq. (6), the Fresnel number is independent of the lasant half-width and is given by $F=(\lambda/2\lambda_x)\ln 2$, where $\lambda$ is the wavelength of the driving laser. For Li-like Ne at 98 Å driven by a 0.25-$\mu$m laser, one has approximately 80 modes. An input energy of 100 mJ and a total efficiency of $5\times10^{-5}$ gives only 0.06 $\mu$J of coherent output energy per pulse. The fraction of coherent energy can be increased by matching $z$ with $L_{sat}$, thereby exploiting gain discrimination effects associated with the strongest growing transverse modes. However, the largest efficiencies (as shown in the next section) occur when $z$ considerably exceeds a saturation length. The amount of coherent energy can be increased by mode selection which delays saturation and allows a selected number of modes to grow exponentially over a longer length. For example, plasma transverse electron density gradients can contribute to refractive defocusing of the weakly growing modes thereby reducing the number of modes. To determine the increase in coherent energy this process requires the shape and slope of the electron density profile as a function of $z$ and is beyond the scope of this paper. The output from an optical-field-induced plasma x-ray laser is estimated to have good longitudinal coherence and relatively poor transverse coherence but improvements in transverse coherence are possible.

## IV. LITHIUMLIKE NEON RESULTS

We discuss the energy efficiencies that can be obtained from optical-field-ionized plasma x-ray lasers for the case of lasing in Li-like Ne. We show what laser intensities are required to sufficiently empty the lower laser state during field ionization. In addition, we study the scaling of gain, saturation length, duration of gain, saturation intensity, and energy efficiency with electron temperature and density. We concentrate on the $3d_{5/2}$-$2p_{3/2}$ fine-structure transition in Li-like Ne at 98 Å. Shell-averaged atomic data are used to determine the populations of the $n=2$, 3, 4, etc., levels of Li-like Ne as a function of time with given initial plasma conditions following the ionization. The sublevels, e.g., $3d_{5/2}$ and $2p_{3/2}$, are assumed populated according to their statistical weights, but the oscillator strength, linewidth, and energy of the fine-structure transition are used to calculate the gain coefficient. Details of the atomic physics calculation are given in the next section.

The $3d_{5/2}$-$2p_{3/2}$ transition has the largest gain coefficient of the fine-structure transitions connecting the $n=3$ level to the $n=2$ ground-state level as shown in Fig. 1. The time dependence of the shell-averaged $n=3$ to 2 gain coefficient along with the gain coefficients for three fine-structure transitions with largest gains are given for an electron temperature of 40 eV and electron density of $5\times10^{20}$ cm$^{-3}$ following ionization. The shell-averaged gain is a valid estimate of gain only when the energy difference between the fine-structure transitions is small compared to the linewidth. This is rarely the case for the ions of interest. The $3d_{5/2}$-$2p_{3/2}$ transition has a maximum gain coefficient of 127 cm$^{-1}$ approximately 0.3 psec after the ionization to He-like Ne with a FWMH gain duration of 0.43 psec.

The calculation of gain assumes that the lower laser state is initially empty following the ionizing pulse. The very large ionization rates calculated for field ionization make this a reasonable assumption provided the intensity of the ionizing laser is sufficiently high. The tunneling ionization theory of Ammosov, Delone, and Krainov [14] gives an ionization rate from Li-like Ne to He-like Ne of $10^{15}$ sec$^{-1}$ at an intensity of $3\times10^{17}$ W/cm$^2$. The rates of Ammosov *et al.* are larger than those given by some other theories [8], but have been shown to be in good agreement with the experimental data of Augst *et al.* [15] for field ionization of xenon. Augst *et al.* found the rates of Ammosov *et al.* to be high for the lower ionization stages of neon. However, recent measurements by Perry [16] find good agreement with the rates of Ammosov *et al.* for ionizing neon to the He-like ionization stage. Using the rates of Ammosov *et al.* we calculate the fraction of the population remaining in the $n=2$ ground state of Li-like Ne following ionization. We use a sech$^2$ temporal dependence for the intensity centered around

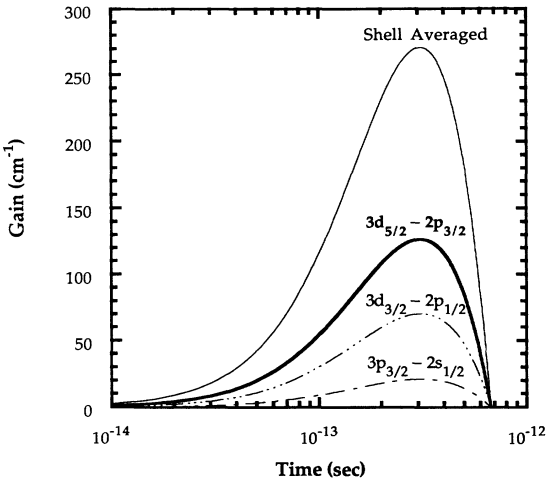


FIG. 1. The time dependence of the shell-averaged (neglecting fine structure) $n=3$ to 2 gain coefficient in Li-like Ne along with the gain coefficients for three fine-structure transitions with the largest gains for plasma conditions of $T_e=40$ eV and $n_e=5\times10^{20}$ cm$^{-3}$ following ionization.

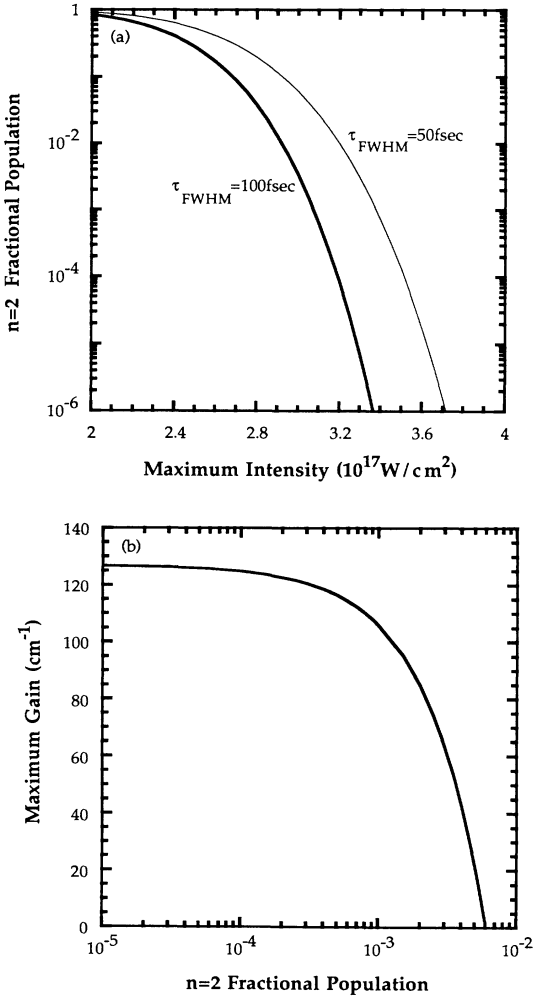


FIG. 2. (a) The $n=2$ fractional population following field ionization as a function of intensity for laser pulses with FWHM durations of 50 and 100 fsec. (b) The calculated $3d_{5/2}$-$2p_{3/2}$ gain coefficient vs fractional population in the $n=2$ levels following ionization.

$\tau=0$ with a FWHM duration of $\tau_{\rm FWHM}$: $I(\tau)=I_{\rm max}{\rm sech}^2[2\ln(\sqrt{2}+1)\tau/\tau_{\rm FWHM}]$. The $n=2$ fractional population as a function of $I_{\rm max}$ is given in Fig. 2(a) for $\tau_{\rm FWHM}=50$ and 100 fsec. The calculation assumes that there is no recombination during the pulse. In the absence of an ionizing electric field we calculate that less than $10^{-4}$ ions would recombine and have an electron in the $n=2$ levels during a 100-fsec period. Recombination occurs primarily into the upper states followed by a collisional cascade to the lower levels. The ionizing electric field of the laser can easily remove the electrons from the upper states which greatly inhibits the filling of the lower levels during the pulse.

In Fig. 2(b) we show the effect of an initial population in the $n=2$ levels on the calculated $3d_{5/2}$-$2p_{3/2}$ gain coefficient. If the $n=2$ fractional population is less than $10^{-4}$, there is only a very small decrease in the gain compared with assuming an initially empty lower laser level. If the $n=2$ fractional population is greater than $10^{-3}$, the gain is significantly reduced with no gain predicted for a fractional population greater than $6\times10^{-3}$. In determining the input energy we require that the fractional population be less than $10^{-4}$ and for a 100-fsec pulse this implies that $I_{\rm max}\geq 3.2\times10^{17}$ W/cm$^2$ in the lasing medium. A 50-fsec pulse would require only a slightly higher intensity.

The saturation intensity for an electron temperature of 40 eV and electron density of $5\times10^{20}$ cm$^{-3}$ is $1.0\times10^{11}$ W/cm$^2$. The saturation length is weakly dependent on the radius of the lasing channel with $L_{\rm sat}=0.11$ and 0.09 cm for $a=5$ and 10 $\mu$m, respectively. In contrast, the energy efficiency has a strong scaling with radius primarily from the $a^2$ scaling in $L_{\rm cf}$, Eq. (6). We calculate $\eta=1.7\times10^{-6}$ and $7.8\times10^{-6}$ for $a=5$ and 10 $\mu$m, respectively. All of the efficiencies we present in this paper use a 100-fsec driving pulse to calculate the input energy. As discussed in Sec. VI, in order to obtain this choice of initial conditions, i.e., $T_e=40$ eV and $n_e=5\times10^{20}$ cm$^{-3}$, a driving pulse of less than 100 fsec may be required to control heating associated with Raman backscatter. In addition to the rapid scaling of efficiency with radius, we also find rapid scaling with electron temperature and density.

We first study the scaling with electron temperature of the quantities that enter into the calculation of the efficiency. The maximum small-signal-gain coefficient $G_{\rm max}$ for the $3d_{5/2}$-$2p_{3/2}$ transition as a function of temperature is shown in Fig. 3(a). The gain decreases from values above 100 cm$^{-1}$ for low temperatures to 13 cm$^{-1}$ at $T_e=100$ eV. An increase in temperature results in a slower recombination from He-like Ne to Li-like Ne, and the slower filling of the excited levels results in smaller population inversions and gains. The dependence of $G_{\rm max}$ on $T_e$ is very well approximated by a power law: $G_{\rm max}\sim T_e^{-2.6}$. The value of the gain affects the efficiency through $L_{\rm sat}$, Eq. (7). The saturation gain length product is usually not very sensitive to plasma conditions. We do find a weak dependence of $G_{\rm max}L_{\rm sat}$ on $T_e$ as shown in Fig. 3(a) for a plasma radius of 5 $\mu$m. The values range from around 10 for low temperatures and increases to approximately 20 for $T_e=100$ eV with a $T_e^{0.5}$ scaling. These scalings of $G_{\rm max}$ and $G_{\rm max}L_{\rm sat}$ combine to give $L_{\rm sat}\sim T_e^{3.1}$. For a saturated laser, the other two important quantities in determining the scaling of energy efficiency with plasma conditions are the saturation intensity and the duration of the gain. The dependencies of these quantities with $T_e$ are shown in Fig. 3(b). The modest increase in $I_{\rm sat}$ with increasing temperature is a result of a larger $\gamma_{\rm out}$ entering Eq. (2) associated with faster electron collisional rates out of the lasing levels. Fitting the $I_{\rm sat}$ curve with a power law, we obtain $I_{\rm sat}\sim T_e^{0.6}$. The FWHM duration of the gain $\Delta t$ is almost independent of electron temperature with a $T_e^{-0.1}$ scaling. Using that the efficiency for a saturated laser scales with $I_{\rm sat}L_{\rm sat}^{-1}\Delta t$ and that these quantities are fit reasonably well by power laws, we expect that the scaling of the efficiency can be approximated by a power law with

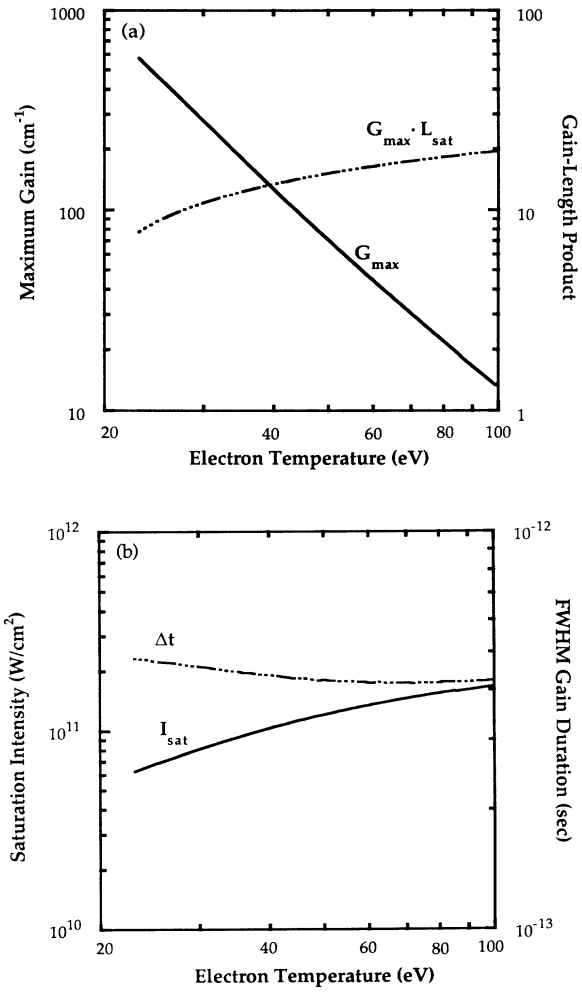


FIG. 3. (a) The maximum gain for the $3d_{5/2}$-$2p_{3/2}$ transition and the product of this gain and the saturation length (for $a=5$ $\mu$m) as a function of electron temperature for an electron density of $5\times10^{20}$ cm$^{-3}$. (b) The saturation intensity and the FWHM duration of the gain as a function of electron temperature for an electron density of $5\times10^{20}$ cm$^{-3}$.

TABLE I. The exponent $x$ in the power-law scaling of the energy efficiency $\eta$, and the quantities that enter in the calculation of $\eta$, with the electron temperature $\sim T_e^x$ and the electron density $\sim n_e^x$. A value of $a=5$ $\mu$m is used to obtain $L_{sat}$ and $\eta$. For the $T_e$ scaling, we take $n_e=5\times10^{20}$ cm$^{-3}$ and for the $n_e$ scaling, we take $T_e=40$ eV.

| Scaling | $G_{max}$ | $G_{max}L_{sat}$ | $L_{sat}$ | $I_{sat}$ | $\Delta t$ | $\eta$ |
|---|---|---|---|---|---|---|
| $T_e$ | −2.6 | +0.5 | +3.1 | +0.6 | −0.1 | −2.6 |
| $n_e$ | +1.5 | −0.1 | −1.6 | +1.7 | −0.6 | +2.7 |

$\eta\sim T_e^{-2.6}$. This scaling is shown in Fig. 4 for two values of plasma radius. As the temperature increases, the saturation length increases until it exceeds $L_{cf}$ for a given plasma radius. After this point there is a very rapid drop in efficiency with increasing temperature which can be seen in the figure as a sudden change in slope. Efficiencies greater than $10^{-5}$ are calculated for $a=10$ $\mu$m provided that $T_e\leq35$ eV. Figure 4 also shows the scaling of $L_{sat}$ with temperature for $a=5$ and 10 $\mu$m. The various scalings with electron temperature are summarized in Table I.

In contrast with the scaling with electron temperature, $I_{sat}$ and $L_{sat}$ contribute a comparable amount to the scaling of efficiency with electron density and in the same direction, i.e., $I_{sat}\sim n_e^{1.7}$ and $L_{sat}^{-1}\sim n_e^{1.6}$. Figure 5 gives the dependence of $G_{max}$, $L_{sat}$, $I_{sat}$, and $\Delta t$ with $n_e$ for $T_e=40$ eV and $a=5$ $\mu$m. An increase in $I_{sat}$ with $n_e$ occurs because of an increase in $\gamma_{out}$ from the faster electron collisional rates at the higher densities. The decrease in $L_{sat}$ with an increase in $n_e$ is because of the increase in the gain coefficient as a result of the higher density and faster collisional filling of the upper laser state. The gain length product is nearly constant with a $n_e^{-0.1}$ scaling. The decrease in gain duration with an increase in $n_e$ is because the lower laser state is being filled through electron collisions in addition to the radiative contribution. The scaling of gain duration with $n_e$ is approximately $\Delta t\sim n_e^{-0.6}$. These scalings combine to give $\eta\sim n_e^{2.7}$ and are summarized in Table I. The dependence of efficiency on $n_e$ is shown in Fig. 6 for a range of electron temperatures and a plasma radius of 5 $\mu$m.

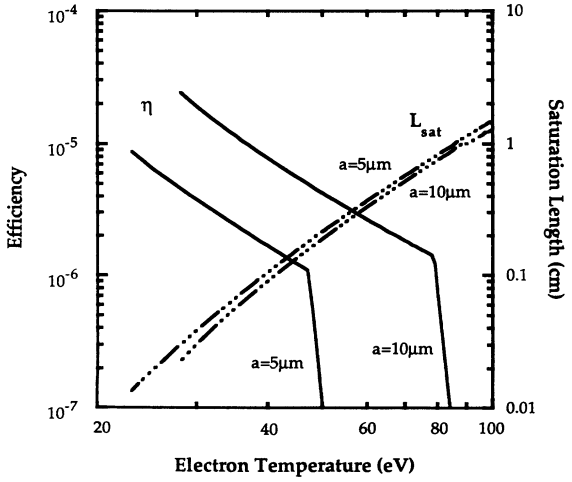


FIG. 4. The energy efficiency and saturation length in Li-like Ne as a function of electron temperature for different values of plasma radius $a$ and an electron density of $5\times10^{20}$ cm$^{-3}$.

## V. DETAILS OF ATOMIC PHYSICS CALCULATIONS

The efficiencies calculated for the $3d_{5/2}$-$2p_{3/2}$ transition in Li-like Ne use a simple kinetic model combined with shell-averaged atomic data. The kinetic model ex-

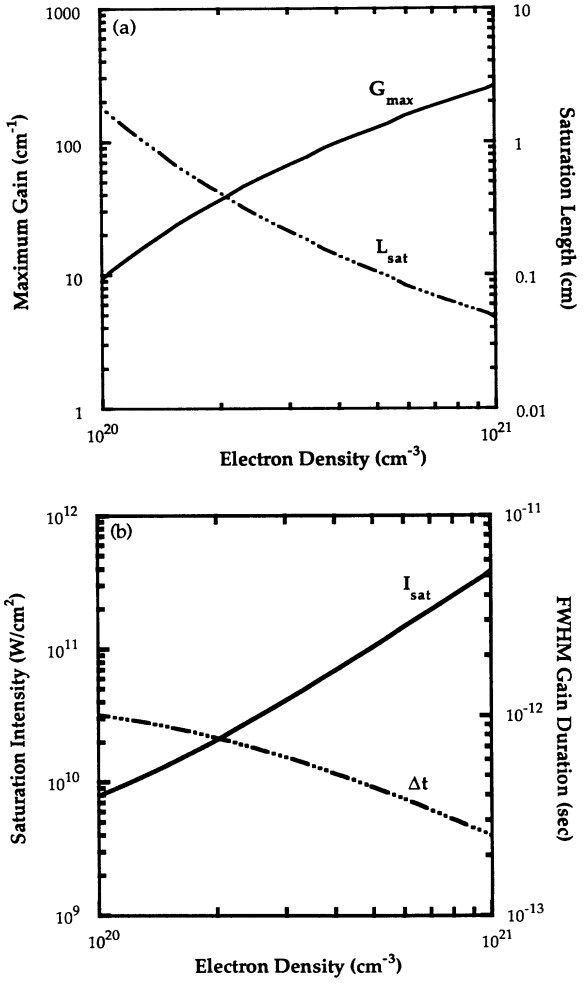


FIG. 5. (a) The maximum gain for the $3d_{5/2}$-$2p_{3/2}$ transition and the saturation length (for $a=5$ $\mu$m) as a function of electron density for an electron temperature of 40 eV. (b) The saturation intensity and the FWHM duration of the gain as a function of electron density for an electron temperature of 40 eV.

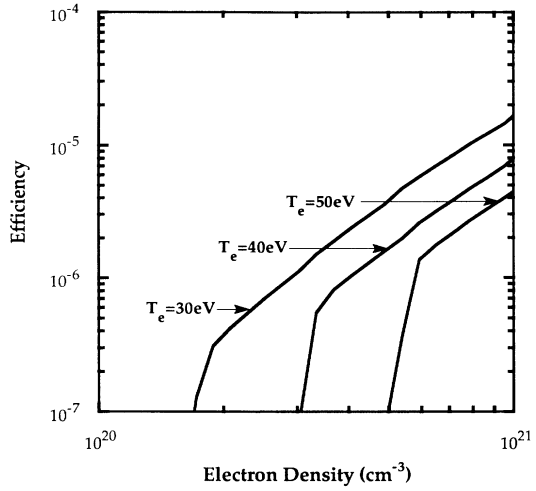


FIG. 6. The energy efficiency in Li-like Ne as a function of electron density for a range of electron temperatures and a plasma radius of 5 $\mu$m.

ploits the three different time scales inherent to the recombination phase following field ionization. The use of shell-averaged atomic data requires that the populations of the sublevels, in a given shell corresponding to a principle quantum number, be proportional to the statistical weights of each sublevel. This approximation is also used to obtain $I_{sat}$ once the populations are determined by the kinetic calculation. We briefly describe the kinetic model and discuss the appropriateness of using shell-averaged atomic data.

There are three distinct time scales in the recombination of a plasma following field ionization by a short-pulse laser. The upper states ($n>4$) come into Saha equilibrium in a very short time ($<50$ fsec) following the pulse. The period of population inversion and lasing down to the ground state occurs over a longer time scale which is limited by spontaneous radiative rates to be of order 1 psec. The time over which significant recombination to the next lower ionization state occurs ($>100$ psec) is the longest time scale. We are primarily interested in the intermediate time scale and treat the time scale for Saha equilibration in the upper levels as instantaneous. The number of upper levels is determined by continuum lowering [17]. Because of the short duration of lasing compared to the recombination time out of the ground state to the next lower ionization stage, we assume that all electrons reaching the ground state accumulate in that state. We use these assumptions in a conveniently simple atomic kinetic model that gives good agreement with results from our complete kinetic simulations.

The kinetic calculations assume that the ground state of Li-like Ne is initially empty. We have studied the effect of initial population on gain and find that for an initial population greater than 0.1% of the total ions in the ground state of Li-like Ne the gain is significantly reduced. Very complete emptying of the ground state is a feature of optical-field-induced ionization and the observation of lasing will provide strong evidence of such emptying.

The appropriateness of using shell-averaged atomic data is addressed by comparing results with those obtained using a detailed atomic model which allows independent sublevels. We find that two processes that can cause sublevels to not be populated according to their statistical weights act in opposite directions and largely cancel. The first arises when the energy differences between the sublevels is of the order of the electron temperature. The second occurs when a given fine-structure transition becomes saturated and a large fraction of the population flow between shells is carried by that transition.

The assumption that the sublevels are populated according to their statistical weights is based upon $\Delta E_{max} \ll kT_e$, where $E_{max}$ is the maximum energy difference between any of the sublevels. For a finite energy difference between the sublevels, there is also a Boltzmann factor $e^{-\Delta E/kT}$ that enters into the calculation of the sublevel populations. In the following discussion, we restrict our attention to Li-like Ne but the conclusions are similar for other atomic elements. In the $n=3$ level, the largest $\Delta E$ is between the $3s_{1/2}$ and $3d_{5/2}$ sublevels with a value of 6 eV. (The $3p$ and $3d$ sublevels differ by only 1.5 eV). The energy differences are larger in the $n=2$ level with the $2p_{3/2}$ and $2p_{1/2}$ sublevels having energies approximately 16 eV greater than the $2s_{1/2}$ sublevel. The Boltzmann factor for this value of $\Delta E$ is 0.7 for a representative temperature from Fig. 4 of 40 eV. The $n=2$ shell is primarily populated by radiative transitions into the $2p$ sublevels from the $3d$ sublevels. The $2s$ sublevel is populated radiatively from the $3p$ sublevels and collisionally from the $2p$ sublevels. The electron collision rate between $2p_{3/2}$ and $2s$ is approximately a factor of 2 larger than that between $2p_{1/2}$ and $2s$. Ion collisions are included in our calculations but do not play an important role. These $\Delta n=0$ collisions try to keep a Boltzmann population distribution among the sublevels. The result of all these processes is that at the time of maximum gain the $2p_{3/2}$ level is slightly underpopulated compared with the other $n=2$ levels accounting for statistical weights but not as much as predicted by the Boltzmann factor. The $3d_{5/2}$-$2p_{3/2}$ transition has a slightly higher small-signal gain ($\approx 5-10\%$) when sublevels are treated independently primarily because of the reduced $2p_{3/2}$ population giving a larger inversion ratio.

The other effect we consider selectively increases the population of the $2p_{3/2}$ sublevel when the lasing intensity approaches the saturation intensity. The $3d_{5/2}$-$2p_{3/2}$ transition selectively populates the $2p_{3/2}$ level because a large fraction of the population flow between the $n=3$ and 2 levels passes through this transition. We find that the saturated gain using independent sublevels is nearly the same as the saturated gain obtained by assuming that the sublevels are populated statistically. Thus the two effects we describe act in different directions on the $2p_{3/2}$ sublevel. The general conclusion is that the assumption of statistical population between the sublevels is valid and the use of shell-averaged atomic data is appropriate.

## VI. STIMULATED RAMAN SCATTERING

An important electron heating process to consider for optical-field-ionized plasma x-ray laser schemes is associated with the stimulated Raman scattering (SRS) instability. We show that it is possible to avoid significant heating for laser-plasma conditions relevant to lasing in Li-like Ne by using short pulses. Straightforward use of the standard temporal growth rate for the SRS (backscatter) overestimates the heating for a finite driving laser pulse. In this section, we show that a modified growth rate must be used and we also derive a criterion that allows one to estimate when significant heating is expected. This simple estimate is verified through relativistic particle-in-cell (PIC) simulations.

First, we will look at the case of a steady-state interaction where the pump is continuous over all space. The SRS instability arises from the decay of a pump photon into a scattered photon and a plasmon with a temporal growth rate given by [18]

$$\gamma=\frac{kv_{\rm osc}}{4}\left[\frac{\omega_p^2}{\omega_{ek}(\omega_0-\omega_{ek})}\right]^{1/2}, \tag{9}$$

where $v_{\rm osc}$ is the quiver velocity of an electron in the laser field [$v_{\rm osc}({\rm cm/s})=25.6I^{1/2}({\rm W/cm^2})\lambda(\mu{\rm m})$], $\omega_0$ is the frequency of the incident (pump) laser, and $\omega_p$ is the plasma frequency. The wave number at which the growth rate for direct backscatter maximizes is $k_0+k_0(1-2\omega_p/\omega_0)^{1/2}$. We are interested in electron densities significantly below critical density (i.e., $\omega_0\gg\omega_p$) and use $k\approx 2k_0$. The frequency $\omega_{ek}$ of the plasma wave is given by the dispersion relation $\omega_{ek}^2=\omega_p^2+3k^2v_e^2$, where $v_e$ is the thermal velocity of the background plasma. For our plasma conditions, we can neglect the second term in the dispersion relation and the growth rate for Raman backscatter can be written as

$$\gamma_0=\frac{1}{2}\frac{v_{\rm osc}}{c}\left[\frac{\omega_p/\omega_0}{(1-\omega_p/\omega_0)}\right]^{1/2}\omega_0 . \tag{10}$$

For this case of an infinitely long pump, the plasma waves (as well as the scattered light waves) will grow until they nonlinearly saturate, usually by trapping large numbers of electrons which take energy from the wave. This results in the particles gaining kinetic energy, which translates to an increase in the temperature of the plasma. However, if the pump is finite in extent, the plasma waves may never reach nonlinear saturation, but instead grow up to some lower level and stop.

For a finite pump, one must use a modified growth rate to correctly determine the amount of SRS related heating. To show this, we will write the coupled mode equations that describe the instability in terms of the response of each wave where $a_1$ is the response of the scattered light wave, and $a_2$ is the response associated with the small density perturbation in the plasma which has an electron density $n_e$. The equations to be solved are

$$\left[\frac{\partial}{\partial\tau}-v_{gs}\frac{\partial}{\partial x}\right]a_1=\gamma_0(x-v_0\tau)a_2 ,$$

$$\left[\frac{\partial}{\partial\tau}-v_{gp}\frac{\partial}{\partial x}\right]a_2=\gamma_0(x-v_0\tau)a_1 ,$$

where we have included the finite nature of the pump by taking the growth rate to be a function of $x-v_0\tau$, $v_{gs}$ is the group velocity of the scattered light wave, $v_{gp}$ is the group velocity of the plasma wave, and $v_0$ is the velocity of the pump wave. We consider a pulse of total length $\tau_p$, which is short enough so that saturation does not occur during the pulse. The solution to this set of coupled equations is that the final state for both the scattered light wave $a_{1f}$, and the plasma density perturbation $a_{2f}$ can be written in terms of initial noise levels, $a_{1i}$ and $a_{2i}$, respectively,

$$a_{1f,2f}=a_{1i,2i}\exp\left[\frac{v_0\int_0^{\tau_p}\gamma_0(\tau')d\tau'}{[(v_0+v_{gs})(v_0-v_{gp})]^{1/2}}\right],$$

where $\tau'=x-v_0\tau$. In the limit that the plasma density is well below quarter critical, the group velocities of the scattered light wave and the pump wave are approximately $c$, while that of the plasma wave is negligible. Therefore the growth is approximately

$$a_{1f,2f}=a_{1i,2i}\exp\left[\frac{1}{\sqrt{2}}\int_0^{\tau_p}\gamma_0(\tau')d\tau'\right] . \tag{11}$$

The total growth is found simply by integrating over the growth rate, which contains the spatial dependence of the pump. Notice that the total growth is less than the long-pulse homogeneous plasma case by a factor of $1/\sqrt{2}$.

In the PIC simulations, discussed below, we use a time dependence for the pulse given by $I(\tau)=I_{\rm max}(1-4\tau^2/\tau_p^2)$ for times between $-\tau_p/2<\tau<\tau_p/2$. The growth rate $\gamma_0(\tau)$ in Eq. (11) would have this same time dependence. We restrict our attention to this particular time dependence, but similar results would be obtained by using other choices such as $\mathrm{sech}^2(\tau/\tau_p)$, or $\exp(-\tau^2/\tau_p^2)$ for a Gaussian profile. Putting our time dependence in Eq. (11) and then integrating over the entire pulse length, we obtain

$$a_{1f,2f}=a_{1i,2i}\exp\left[\frac{\sqrt{2}}{3}\gamma_{0\rm max}\tau_p\right],$$

where $\gamma_{0\rm max}$ is defined to be the growth rate given in Eq. (10), where the intensity is taken to be $I_{\rm max}$. The energy density in the plasma waves following the pulse is proportional to $|a_{2f}|^2$. We expect that if the plasma has an initial total energy density of $U_{\rm tot}=\frac{3}{2}nT_e$, then the electron temperature should increase when the energy density of the unstable modes (i.e., $k$ near $2k_0$) approaches $U_{\rm tot}$. Therefore we obtain the following criterion that must be satisfied for a substantial modification of the bulk plasma temperature to occur:

$$U_{\rm tot}\sim U_{ki}\exp\left[\frac{2\sqrt{2}}{3}\gamma_{0\rm max}\tau_p\right] .$$

Here, $U_{ki}$ is the energy density in the most unstable modes near $2k_0$ initially present in the plasma before the pump is sent into the plasma. This can be rewritten as a

criterion on how short a pulse must be, given a particular laser intensity and initial plasma temperature and density, if no heating due to SRS backscatter is required. We express this criterion in terms of the FWHM duration of the intensity, $\tau_{\rm FWHM}=\tau_p/\sqrt{2}$, as

$$\gamma_{0\max}\tau_{\rm FWHM}\leq\tfrac{3}{4}\ln\left[\frac{U_{\rm tot}}{U_{ki}}\right]. \tag{12}$$

If this inequality is satisfied, little or no heating is expected to occur. Using that the wave number range of unstable modes $dk\sim\gamma_0/c$, the ratio of $U_{\rm tot}$ to $U_{ki}$ is expected to be $10^7-10^8$ [5]. Typically, the ratio is smaller ($\sim10^5$) for our PIC simulations because of the finite number of particles and limitations on the grid size. Putting these ratios into the criterion given by Eq. (12), we find that the product $\gamma_{0\max}\tau_{\rm FWHM}$ should be kept below 9 for the simulations, or below 12–14 if the thermal noise estimate of $U_{ki}$ is used.

A series of computer simulations has been performed to check the theory concerning the instability. We used a relativistic PIC code, ZOHAR [19], which includes one spatial dimension (the $z$, or longitudinal dimension) and two velocities (the longitudinal $v_x$, and the transverse $v_z$ which is the direction of the laser electric field). In all cases, the laser is injected from the left boundary, and absorbed at the right. The laser is chosen to have $\lambda=0.25$ $\mu$m and FWHM pulse durations varying between 50 and 100 fsec. The electron distribution is taken to be a Maxwellian at $t=0$, with an initial temperature of 25 eV. The final temperature of the plasma is measured after the pump wave exits the system. This is because the oscillatory motion of the electrons in the laser electric field (transverse to the propagation direction of the laser) is so large in the presence of the pulse that it dominates the energy distribution. However, the majority of this energy is given back to the laser as it passes through the system. The heating associated with this transverse motion (self-consistently included in the simulation) is negligible. The theories regarding the reduced growth rates, and the point at which the temperature of the plasma increases due to SRS electron heating, are both confirmed by the simulations. As a particular example, Fig. 7 shows the final electron distribution for the case of a plasma with an electron density of $5\times10^{20}$ cm$^{-3}$ and a laser pulse with a maximum intensity of $2\times10^{17}$ W/cm$^2$. The $\gamma_{0\max}\tau_{\rm FWHM}$ parameters are 15, 11 and 8 for the 100-, 75-, and 50-fsec pulses, respectively. These results confirm the criterion [Eq. (12)] that if $\gamma_{0\max}\tau_{\rm FWHM}\leq9$, little electron heating from SRS is expected. Additionally, the intensity of the backscattered light (whose growth is identical to that of the energy deposited in the plasma waves, which ultimately goes into heating the electrons) is shown to grow at the rate predicted by Eq. (11), thus confirming that the growth rate is reduced by the factor $1/\sqrt{2}$.

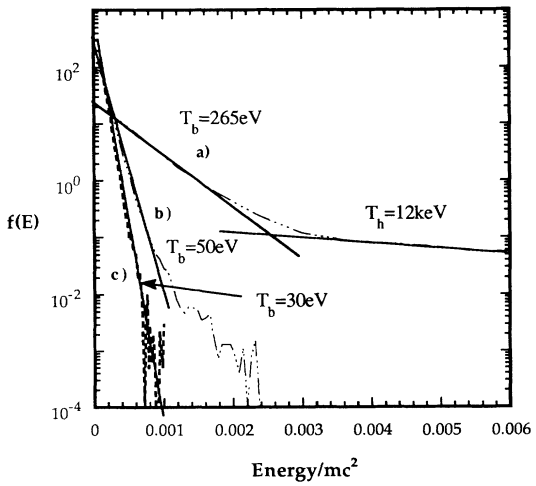


FIG. 7. Energy distribution plot of plasma electrons after the pump laser has passed through the system showing the electron heating as a result of Raman backscattering. The plasma density is $5\times10^{20}$ cm$^{-3}$ and the maximum laser intensity of the pump is $I_{\max}=2\times10^{17}$ W/cm$^2$. The pulse length is taken to be (a) 100 fsec, (b) 75 fsec, and (c) 50 fsec.

To conclude this section, it is found that the growth rate is reduced from the long-pulse infinite-plasma value. Based on the modified growth rate, a criterion is given for when SRS backscatter begins to heat the background plasma. We show that Raman heating can be controlled for laser-plasma conditions relevant to lasing in Li-like Ne by using short pulses. Our PIC simulation estimates of heating are probably conservative because the initial noise level in the simulations is higher than the thermal noise estimate. However, the maximum intensity of $2\times10^{17}$ W/cm$^2$ used in the PIC simulation is approximately 50% lower than what is required to achieve sufficient ionization as discussed in Sec. IV. Using the lower estimate for the noise, and adjusting for the higher intensity, the requirement on pulse durations is relaxed by approximately 25% compared with the simulation results.

## VII. EXTENDING TO LITHIUMLIKE ALUMINUM

We consider the possibility of extending optical-field-ionized plasma x-ray lasers to wavelengths shorter than 98 Å by using an element with a higher atomic number than Ne. In particular, we study lasing at 52 Å in the $3d_{5/2}$-$2p_{3/2}$ transition of Li-like Al. We calculate significantly lower energy efficiencies in Li-like Al as compared with Li-like Ne for comparable electron densities. A more serious problem is the calculated heating from stimulated Raman scattering associated with the required higher driving laser intensities.

The calculated energy efficiency in Li-like Al as a function of electron temperature is shown in Fig. 8 for two plasma radii at an electron density of $5\times10^{20}$ cm$^{-3}$. Comparing with Fig. 4 for Li-like Ne, there is a significant reduction in the efficiencies. To investigate the factors that enter into the efficiencies, we restrict our attention to an electron temperature of 40 eV, a radius of 5 $\mu$m, and an electron density of $5\times10^{20}$ cm$^{-3}$. For these conditions, the $3d_{5/2}$-$2p_{3/2}$ transition has a maximum gain coefficient of 96 cm$^{-1}$ approximately 0.3 psec after the ionization to He-like Al with a FWHM gain duration

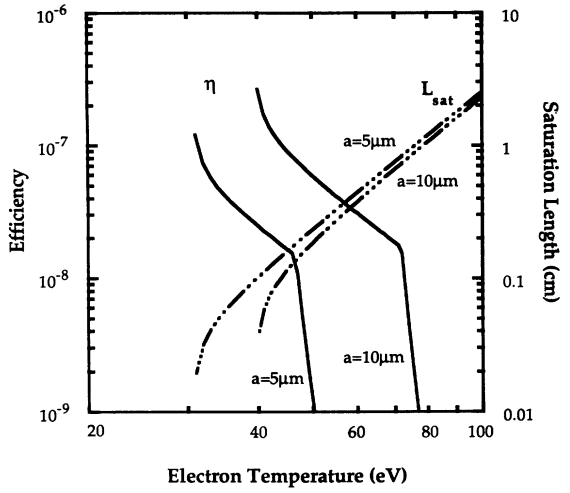


FIG. 8. The energy efficiency in Li-like Al as a function of electron temperature for different values of plasma radius and an electron density of $5\times10^{20}$ cm$^{-3}$.

0.29 psec. The corresponding saturation intensity and length are $1.3\times10^{10}$ W/cm$^2$ and 0.10 cm, respectively. These combine to give an energy efficiency of $2.5\times10^{-8}$. In comparing this value with that obtained in Sec. IV for Li-like Ne for the same initial conditions, we find a decrease in efficiency by a factor of 68. This result shows that a relatively high gain coefficient, of order 100 cm$^{-1}$, does not necessarily lead to a high efficiency.

The differences between Li-like Ne and Li-like Al are summarized in Table II. The maximum gain coefficient is a factor of 1.3 lower in Li-like Al. This decrease in gain occurs despite the faster recombination in Li-like Al. The reason for the decrease in gain is because the spontaneous radiation rates from $n=3$ to 2 are a factor of 3 larger in aluminum leading to a faster filling of the lowest laser level. This faster filling of the ground state results in a shorter duration of lasing with $\Delta t$ being a factor of 1.5 less in Li-like Al. The saturation intensity is smaller for Li-like Al because of a smaller population inversion at the time of maximum gain, a smaller linewidth, and a larger radiative rate. The smaller $I_{\rm sat}$ leads to a slightly smaller $L_{\rm sat}$ for Li-like Al despite the gain coefficient being less. These differences in $L_{\rm sat}$, $I_{\rm sat}$, and $\Delta t$ combined with the factor of 6 higher input energy in Li-like Al associated with the higher required intensity, cf. Eq. (1), explain the lower efficiency in Li-like Al. Efficiencies above $10^{-6}$ are calculated for higher electron densities. However, these higher densities combined with the required higher intensity are calculated to lead to excessive Raman heating.

The stimulated Raman growth rate, Eq. (10), scales approximately as $I^{1/2}n_e^{1/4}$ through $v_{\rm osc}$ and $\omega_p$. The factor of 6 in intensity and a factor of 2 in electron density (to improve efficiency) result in a factor of 3 increase in growth rate in Li-like Al as compared with Li-like Ne. We calculate a bulk electron temperature in Li-like Al greater than 1 keV for an electron density of $1.0\times10^{21}$ cm$^{-3}$ using a 50-fsec pulse. Using a shorter pulse to reduce Raman heating is not practical because there is not sufficient energy in the pulse to ionize the plasma to He-like Al. As discussed in Sec. VI, our calculation of heating is conservative because the initial noise level in the simulation is believed to be larger than would be the case in an experiment. However, an allowance for a possible reduction in the growth rate by $\frac{1}{3}$ to account for this effect is not sufficient to control the heating to allow efficient lasing in Li-like Al. The H-like B scheme at 48 Å of Burnett and Enright [3] requires comparable laser intensities and a similar problem of excessively heating from Raman scattering is predicted.

If the excessive electron heating associated with Raman scattering could be reduced significantly through the use of steep density gradients or larger bandwidth drivers, we find that the efficiency is still much reduced in Li-like Al as compared with Ni-like Ne. This shows the importance of considering factors other than the small-signal-gain coefficient (a 1.3 reduction in gain as compared with a reduction in efficiency by a factor of 68) in determining the appropriateness of a given laser scheme. We believe that a modest reduction in lasing wavelength below 98 Å while maintaining high efficiency is possible for optical-field-ionized plasma x-ray lasers. However, extending the scheme down to wavelength near the carbon $K$ edge ($\sim$45 Å, important for some biological applications of x-ray lasers) is difficult because of reduced efficiencies and excessive Raman heating.

## VIII. DISCUSSION

We have calculated that optical-field-ionized plasma x-ray lasers can be an efficient source of monochromatic x rays. The calculated efficiencies include the reduction in the saturation intensity by accounting for the effect of the lower laser state on saturation. This effect is shown to be larger for H-like ions as compared with Li-like ions. Our calculations of energy efficiency assume that the length of the lasing medium is given by $L_{\rm cf}$ of the ionizing laser. An important issue that needs to be studied both experimentally and theoretically is the propagation of a high-intensity short laser pulse and whether the

TABLE II. The efficiency $\eta$ and the quantities that enter into the efficiency for Li-like Ne and Li-like Al for $T_e=40$ eV, $n_e=5\times10^{20}$ cm$^{-3}$, and $a=5$ $\mu$m.

| Ion | $G_{\rm max}$ (cm$^{-1}$) | $L_{\rm sat}$ (cm) | $I_{\rm sat}$ ($10^{11}$ W/cm$^2$) | $\Delta t$ (psec) | $\eta$ |
|---|---|---|---|---|---|
| Ne | 127 | 0.11 | 1.0 | 0.43 | $1.7\times10^{-6}$ |
| Al | 96 | 0.10 | 0.13 | 0.29 | $2.5\times10^{-8}$ |

beam can remain focused for a confocal length by using a plasma waveguide to control refraction.

We have shown the appropriateness of using shell-averaged atomic data. The two processes that we have studied that can cause the atomic sublevels to not be populated according to their statistical weights act in opposite directions and largely cancel. A further simplification in the kinetics can be made by utilizing the different time scales in the problem. The simple kinetics and the valid approximation that the electron temperature and density do not vary significantly during lasing allows for a straightforward calculation of gain coefficients and other quantities that enter into the calculation of efficiencies. We have exploited the ease of our modeling to explore a wide range of plasma conditions.

In Li-like Ne, the efficiency is found to have nearly power-law scaling with plasma conditions given by $T_e^{-2.6}$ and $n_e^{2.7}$. The rapid scaling with electron temperature and density shows the significant advantage of maintaining low temperatures as the density is increased. Our calculations show that electron heating associated with stimulated Raman scattering can be controlled for the case of Li-like Ne by using short pulses ($\tau_{\mathrm{FWHM}} \leq 100$ fsec) and short wavelength pumps ($\lambda \approx 0.25$ $\mu$m). Experiments designed to measure electron heating as a function of intensity, wavelength, density, and pulse duration would be of major benefit in determining the ions for which lasing following optical-field-induced ionization is possible. Comparable or higher efficiencies are expected for lasing at wavelengths longer than 98 Å (e.g., 173 Å in Li-like O) and can be studied using less energy than required for Li-like Ne.

## ACKNOWLEDGMENTS

We gratefully acknowledge B. Penetrante for discussions on field ionization and N. Bardsley, C. Keane, W. Kruer, A. B. Langdon, R. London, J. Nash, M. Rosen, and E. Williams for many useful suggestions. This work was performed under the auspices of the U.S. Department of Energy by the Lawrence Livermore National Laboratory under Contract No. W-7405-ENG-48.

[1] For a description of most x-ray laser schemes, see R. C. Elton, *X-Ray Lasers* (Academic, San Diego, CA, 1990).
[2] J. Peyraud and N. Peyraud, J. Appl. Phys. **43**, 2993 (1972).
[3] N. H. Burnett and G. D. Enright, IEEE J. Quantum Electron. **QE-26**, 1797 (1990).
[4] P. Amendt, D. C. Eder, and S. C. Wilks, Phys. Rev. Lett. **66**, 2589 (1991).
[5] A. Tünnermann, R. Henking, and B. Wellegehausen, Appl. Phys. Lett. **58**, 1004 (1991).
[6] P.B. Corkum, N. H. Burnett, and F. Brunel, Phys. Rev. Lett. **62**, 1259 (1989).
[7] N. H. Burnett and P. B. Corkum, J. Opt. Soc. Am. B **6**, 1195 (1989).
[8] B. M. Penetrante and J. N. Bardsley, Phys. Rev. A **43**, 3100 (1991).
[9] For recent advances, see *Femtosecond to Nanosecond High-Intensity Lasers and Applications,* edited by E. M. Campbell (SPIE, Bellingham, 1990).
[10] R. A. London, Phys. Fluids **31**, 184 (1988).
[11] A. W. Siegman, *Lasers* (University Science Books, Mill Valley, CA, 1986).
[12] R. W. Lee, J. Quant. Spectrosc. Radiat. Transfer **40**, 561 (1988).
[13] R. A. London, M. Strauss, and M. D. Rosen, Phys. Rev. Lett. **65**, 563 (1990); P. Amendt, R. A. London, and M. Strauss, Phys. Rev. A **44**, 7478 (1991).
[14] M. V. Ammosov, N. B. Delone, and V. P. Krainov, Zh. Eksp. Teor. Fiz. **91**, 2008 (1986) [Sov. Phys.—JETP **64**, 1191 (1986)].
[15] S. Augst, D. D. Meyerhofer, D. Strickland, and S. L. Chin, J. Opt. Soc. Am. B **8**, 858 (1991).
[16] M. D. Perry (private communication).
[17] R. M. More, J. Quant. Spectrosc. Radiat. Transfer **27**, 345 (1982).
[18] W. L. Kruer, *The Physics of Laser Plasma Interactions* (Addison-Wesley, Redwood City, CA, 1988).
[19] A. B. Langdon and B. F. Lasinski, in *Methods in Computational Physics,* edited by J. Killeen *et al.* (Academic, New York, 1976), Vol. 16, p. 327.